Nano Research
DOI 10.1007/s12274-015-0736-8
Research Article
ISSN 1998-0124
CN 11-5974/O4

Three dimensional multimodal sub-diffraction imaging with spinning-disk confocal microscopy using blinking/fluctuation probes

Xuanze Chen†, Zhiping Zeng†, Hening Wang, and Peng Xi (✉)

Nano Res., **Just Accepted Manuscript** • DOI 10.1007/s12274-015-0736-8
http://www.thenanoresearch.com on January 28, 2015

Just Accepted

TSINGHUA UNIVERSITY PRESS Springer

Template for Preparation of Manuscripts for *Nano Research*

This template is to be used for preparing manuscripts for submission to *Nano Research*. Use of this template will save time in the review and production processes and will expedite publication. However, use of the template is not a requirement of submission. Do not modify the template in any way (delete spaces, modify font size/line height, etc.). If you need more detailed information about the preparation and submission of a manuscript to Nano Research, please see the latest version of the Instructions for Authors at http://www.thenanoresearch.com/.

TABLE OF CONTENTS (TOC)

Authors are required to submit a graphic entry for the Table of Contents (TOC) in conjunction with the manuscript title. This graphic should capture the readers' attention and give readers a visual impression of the essence of the paper. Labels, formulae, or numbers within the graphic must be legible at publication size. Tables or spectra are not acceptable. Color graphics are highly encouraged. The resolution of the figure should be at least 600 dpi. The size should be at least 50 mm × 80 mm with a rectangular shape (ideally, the ratio of height to width should be less than 1 and larger than 5/8). One to two sentences should be written below the figure to summarize the paper. To create the TOC, please insert your image in the template box below. Fonts, size, and spaces should not be changed.

Three dimensional multimodal sub-diffraction imaging with spinning-disk confocal microscopy using blinking/fluctuation probes

Xuanze Chen, Zhiping Zeng, Hening Wang, and Peng Xi*

Peking University, China

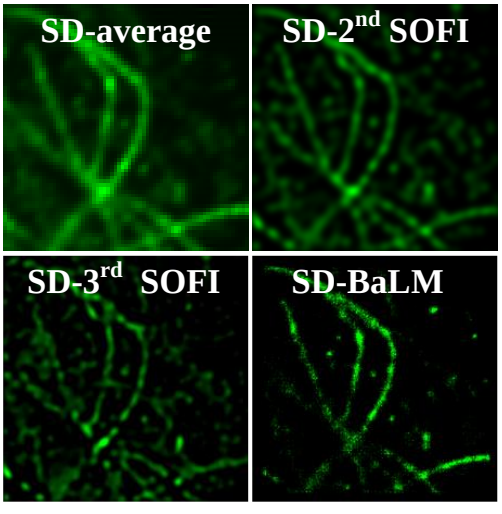

Previous localization super-resolution techniques cannot offer three-dimensional imaging easily. Here we present 3D-MUSIC, which based on spinning-disk (SD) confocal microscopy, offers three-dimensional multimodal sub-diffraction imaging through fluctuation of the fluorescent probe.

Peng Xi, http://bme.pku.edu.cn/~xipeng/

Nano Research
DOI (automatically inserted by the publisher)
Research Article
ISSN 1998-0124
CN 11-5974/O4

Three dimensional multimodal sub-diffraction imaging with spinning-disk confocal microscopy using blinking/fluctuation probes

Xuanze Chen†, Zhiping Zeng†, Hening Wang, and Peng Xi (✉)

Department of Biomedical Engineering, College of Engineering, Peking University, Beijing 100871, China
† *Authors with equal contribution*

Received: day month year
Revised: day month year
Accepted: day month year (automatically inserted by the publisher)

KEYWORDS

multi-modality, super-resolution microscopy, three-dimensional, spinning-disk confocal

ABSTRACT

Previous localization super-resolution techniques cannot offer three-dimensional imaging easily. Here we present a three-dimensional multimodal sub-diffraction imaging with spinning-disk (SD) confocal microscopy, 3D-MUSIC, which not only takes fully advantages of spinning-disk confocal microscopy, such as fast imaging speed, high signal-to-noise ratio, optical-sectioning capability, but also extends its spatial resolution limit along all three dimensions. Both axial and lateral resolution can be improved simultaneously by virtue of the blinking/fluctuation nature of the modified fluorescent probes, exemplified by the quantum dots (QDs). Further, dual-modality super-resolution image can be obtained, by super-resolution optical fluctuation imaging (SOFI), and bleaching/blinking assisted localization microscopy (BaLM). Therefore, fast super-resolution imaging can be achieved with SD-SOFI by only capturing 100 frames, yet a high-resolution imaging can be provided with SD-BaLM.

1 Introduction

Optical fluorescence microscopy has been routinely applied to explore a vast variety of biological phenomena in life sciences [1]. Confocal laser scanning microscopy (CLSM) is one of the most powerful and versatile diagnostic tools in the biomedical science due to its unique ability to eliminate the out-of-focus noise, excellent in three-dimensional (3D) optical-sectioning ability, especially in studying cell biology [2-4]. Different from conventional scanning mode, spinning-disk

Address correspondence to xipeng@pku.edu.cn

(SD) confocal microscopy is a special type of confocal microscope, which uses an array of pinholes arranged spirally, to form parallel scan across the specimen [5]. It enables the utilization of a CCD detector to collect the confocal optical sectioning image from the specimen [6]. However, due to wave nature of light, spatial resolution of CLSM is limited to $1/\sqrt{2}$ times the Rayleigh diffraction limit, determined by the laser wavelength and numeral aperture (NA) [7-10]. Thus, when it comes to unveil intracellular world, conventional CLSM or SD has met grand challenges in discerning fine structures beyond the diffraction limit. As a consequence, a microscopic technique which is able to break the diffraction barrier is highly desirable for further biological research [11-13].

In the past decade, various super-resolution techniques aiming at breaking the diffraction barrier have sprung up [14-18], such as stimulated emission depletion microscopy (STED) [19, 20], saturated structured illumination microscopy (SSIM) [21, 22], photoactivated localization microscopy (PALM) [23, 24], stochastic optical reconstruction microscopy (STORM) [25, 26], bleaching/blinking assisted localization microscopy (BaLM) [27], super-resolution optical fluctuation imaging (SOFI) [28, 29], etc. It should be noted that, as PALM/STORM are based on the localization of a wide field image, 3D super-resolution imaging has to be implemented with sophisticated Point Spread Function (PSF) modulation and following data postprocessing, such as astigmatism [26], double helix [30], etc.

Among these super-resolution techniques [31], BaLM and SOFI are two novel super-resolution microscopy techniques that can both take the advantage of blinking/fluctuation probes to achieve contrast-enhanced super-resolution imaging, but differ in the algorithms: BaLM firstly uses subsequent subtraction for the captured adjacent image frames, then resolves the localization information using single particle localization method; SOFI extracts localization information from the temporal correlation statistics of pixel intensity fluctuations, and the spatial resolution can be enhanced n folds by calculating nth-order cross-cumulant [32].

To obtain better performance of these blinking-based/localization-based super-resolution techniques, original images must be obtained under fast imaging rate simultaneously with high signal-to-noise ratio (SNR) for ensuring the correctness of super-resolution analysis algorithms. The probes which are commonly used, such as quantum dots (QDs) [33, 34], dyes [35] or photoswitchable fluorescent proteins [36, 37], possess the ability of blinking/fluctuation or photoswitchability. Especially, QDs have been widely used as an alternative fluorescent inorganic dye in both cellular and tissue imaging, for its high brightness and photostability [38, 39]. Initially, blinking/ fluctuation was treated as a negative effect and suppressed by surface modification with special reagents. Later, it was utilized as a means for super-resolution imaging [40].

In this paper, we firstly realized the three-dimensional multimodal sub-diffraction imaging based on spinning-disk confocal microscopy using QD fluctuation probes. QDs used in multimodal sub-diffraction imaging with spinning-disk confocal microscopy enables higher SNR and better 3D optical-sectioning ability, which make 3D-MUltimodal Sub-diffraction Imaging with spinning-disk Confocal (3D-MUSIC) microscopy come true. This multimodal sub-diffraction imaging technique allows any z depth of cell to be resolved.

2 Materials and methods

3D-MUSIC can easily achieve the three dimensional super-resolution imaging of subcellular structure labeled with blinking/fluctuation probes across a large field of view simultaneously possessing a good z optical-sectioning capability.

The image collection of the microtubule networks was performed on a spinning-disk confocal fluorescence microscope (PerkinElmer UltraView VoX) with an oil objective (Nikon, 100x, N. A. 1.4). A laser with the wavelength of 405 nm was employed for exciting the fluorescence emission of QD625 (power density: 200 W/cm^2). The fluorescence signals were collected by an EMCCD (Hamamatsu, C9100-13). The exposure time of each frame was 30

ms, and 1000 frames for each slice (200 nm each slice along the z-axis) were captured. In the experiment, drift correction was realized without any fiducial beads. After the acquisition of the time-lapse images, we implemented drift correction with sub-pixel precision based on discrete Fourier transforms and nonlinear optimization [41].

The spatio-temporal cross-cumulants between neighboring pixels are calculated in the SOFI processing [32, 42]. An approximation of the underlying Point Spread Function can be well estimated by calculating the cross-cumulants. Besides, the spatial resolution can be linearly enhanced over cumulant order by using Fourier-reweighting. Additionally, the nonlinear response to brightness and blinking heterogeneities in SOFI processing can be prominently eliminated by analyzing the blinking kinetics of the fluorophores using balanced SOFI. In this work, SOFI processing is performed with the bSOFI software using 100 images [32]. Blinking assisted localization microscopy (BaLM) [27] was implemented by a custom-written Matlab program which is based on 1000 images subtraction. Image subtraction was done by subtracting consecutive images from the acquired image series: $J_i = I_n - I_{n-1}$, where I_n, I_{n-1} represent the captured image frames, J_i represents the subtracted image slice. After subtraction, J_i were combined as an image stack for localization. Finally, single molecule localization was performed on the subtracted image sequences using QuickPALM (ImageJ) [43].

3 Results

3.1 Schematic illustration

In Fig. 1, assuming a test sample labeled with blinking/fluctuation fluorophores, when applying illumination, the fluorophores emit fluorescence intermittently over exposure time. This type of fluorescence intermittency (blinking/fluctuation) can be analyzed by SOFI algorithm to improve the spatial resolution of the captured images. Furthermore, the captured image frames can be subtracted pairwise sequentially, isolating some sparsely distributed blinking events for localization-based super-resolution imaging. Finally, after localizing the individual fluorophores from the subtracted frames, a super-resolution image can be reconstructed using blinking assisted localization microscopy (BaLM).

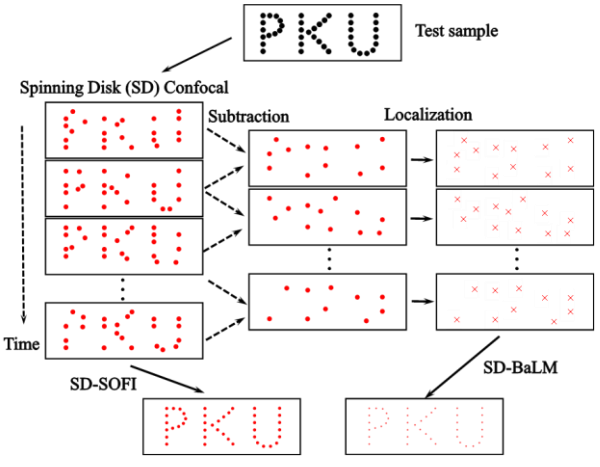

Figure 1 Schematic diagram of multimodal sub-diffraction imaging with spinning-disk confocal microscopy using fluctuation probes.

3.2 Numerical simulations

Labeling density is of great importance in reflecting the structure faithfully in biological fluorescence imaging, especially for super-resolution microscopy [44]. In this simulation, we chose three letters written as "PKU" to be the test object and simulated the blinking process of the fluorophores distributed on the test object under various labeling densities ranging from 5 μm^{-1} to 24 μm^{-1} shown in Fig. 2. Here, the pixel number in the simulation was set to 240*240 with a pixel size of 20 nm. The simulated PSF was calculated based on the emission wavelength of the QDs and the numerical aperture of the objective. In general, the FWHM of the PSF is given by the Abbe diffraction equation:

$$d \approx \frac{0.51\lambda}{N.A.}.$$

The peak emission wavelength of QD625 used in our experiment is 625 nm, with the N.A. of the objective of 1.4. Therefore, the FWHM of the PSF is approximately 228 nm. The blinking process was simulated by generating 1000 frames of blinking fluorophores on the test object. The blinking of each point obeys a rate ratio r of 5, i. e.

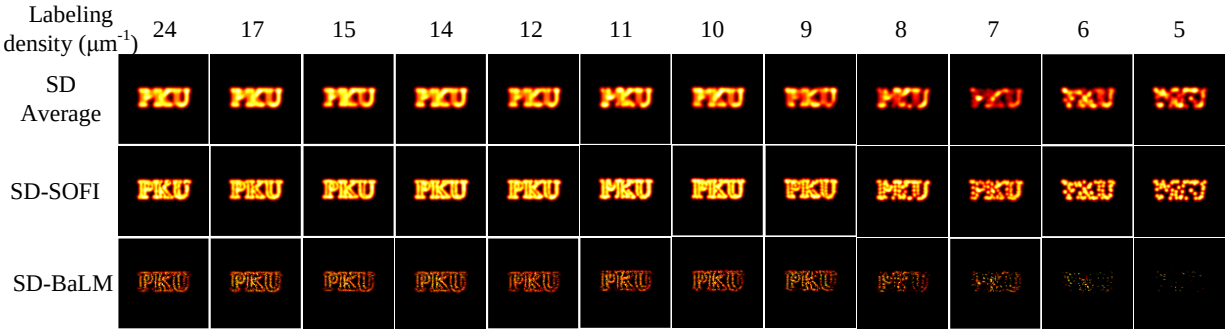

Figure 2 Numerical simulations of average, SD-SOFI (3rd cumulant) and SD-BaLM images under different labeling densities.

$$r = \frac{t_{off}}{t_{on}},$$

which means that the blinking off time is 5-fold that of the blinking on time statistically. After simulation, the averaged, SD-SOFI and SD-BaLM images were reconstructed using bSOFI and custom-written BaLM algorithms (Matlab, MathWorks). When the labeling density is low (i.e., < 7 μm^{-1}), the complete structure of the test image cannot be reconstructed after SD-SOFI and SD-BaLM processing. SD-SOFI have generated the results with severe discontinuities. In particular, SD-BaLM totally fails to present structurally observable results. When increasing the labeling densities, the integrity of the test image can be well maintained both in SD-SOFI and SD-BaLM processing. However, if the labeling densities are excessively high (typically over 14 μm^{-1}), high order SD-SOFI processing has undesirably induced artifacts.

Unlike PALM/STORM techniques, which typically discard data from molecules with overlapping images, dominant overlapping events are allowed in our simulation. As can be seen, the test object was blurred in the averaged image displayed in Fig. 2. This is due to insufficient spatial resolution in spinning-disk confocal microscopy. Whereas, by applying SD-SOFI processing, the detailed structures of the test object can be clearly discerned. This demonstrates that SD-SOFI has the capability of reconstructing sub-diffraction images even when the overlapping events are dominant. Subsequently, SD-BaLM was introduced for achieving single molecule localization microscopy based on image subtraction. 2000 frames were generated for blinking assisted localization. After localization and image reconstruction, the resolution can be further improved compared to both SD average and SD-SOFI counterparts. Correlation coefficients of the target image with the average, SD-SOFI and SD-BaLM was shown in Fig. S1.

To test the noise resistance and robustness of the proposed multimodal method, a random noise was taken into consideration in Fig. S2.

3.3 Super-resolution imaging based on spinning-disk confocal microscope

The microtubules in COS7 cells were labeled by QD625 with the labeling density of 17 μm^{-1} in our experiment. A laser with a wavelength of 405 nm was applied for fluorescence excitation. A spinning-disk confocal microscope was utilized for super-resolution imaging which was achieved by virtue of the blinking/fluctuation behavior of QDs. During the experiment, one thousand conventional spinning-disk confocal images were collected for reconstructing a super-resolution image. In Fig. 3(a), the collected one thousand images were superimposed, generating an average image of the microtubule networks. After 2-3 order SOFI processing, the background noise was well suppressed and the SNR has been significantly improved. The intensity plot in Fig. 3(e) indicates that the FWHMs for spinning disk confocal microscopy and 3rd order SD-SOFI are 390 nm and 180 nm, respectively. Here the fluorescence emission central wavelength is 625 nm, and an objective with N.A.=1.4 is employed, so the theoretical resolution is ~228 nm. For spinning disk microscopy, the resolution is generally larger than the theoretical

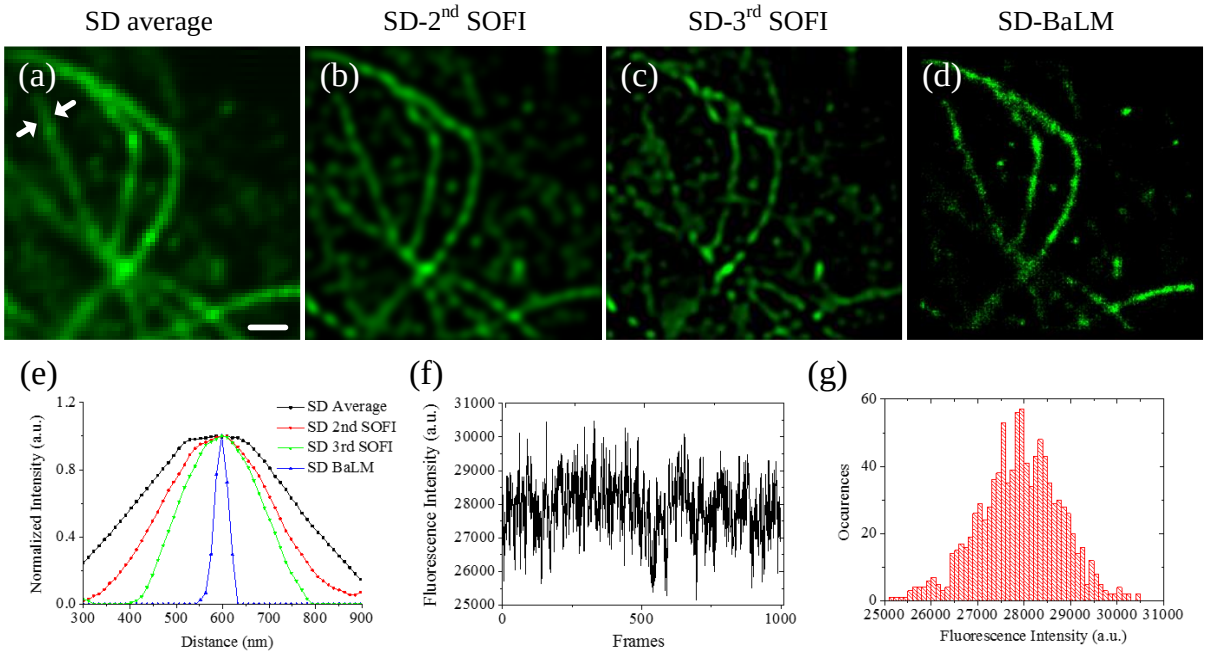

Figure 3 (a) Average, (b) 2nd and (c) 3rd SOFI super-resolution imaging of 100 frames based on spinning-disk confocal microscope (SD); (d) The SD-BaLM is based on the 2000 frames subtracted from original 1000 image data; (e) Intensity profile of cross-sections along the white arrow as indicated in the upper panels; (f) The intensity fluctuation of single pixel in SD microscopy and (g) The histogram distribution of (f). Scale bar: 1 μm.

prediction because the objective aperture is not filled, and the confocal pinhole is relatively large. Benefitted from the localization process, SD-BaLM can improve the resolution to 40 nm in our experiment. The intensity fluctuation of single pixel in SD microscopy was presented in Fig. 3(f) and its Poisson blinking intensity statistics distribution shown in Fig. 3(g) indicates that QDs does not suffer from the higher order analysis [45].

3.4 Three-dimensional Super-resolution imaging based on spinning-disk confocal microscope.

The axial resolution r_z of conventional far-field microscopy is always limited by the diffraction to more than 600 nm, which can be mathematically described by the following equation [46]:

$$r_z = \frac{2n\lambda}{NA^2},$$

where λ is the average wavelength of illumination laser, n is the refractive index of the immersion medium, and NA is the numerical aperture of the objective. For confocal microscopy, as the focused excitation laser is coupled with pinhole-restricted detection, in principle the axial resolution can be improved by up to a factor of 1.4 [46].

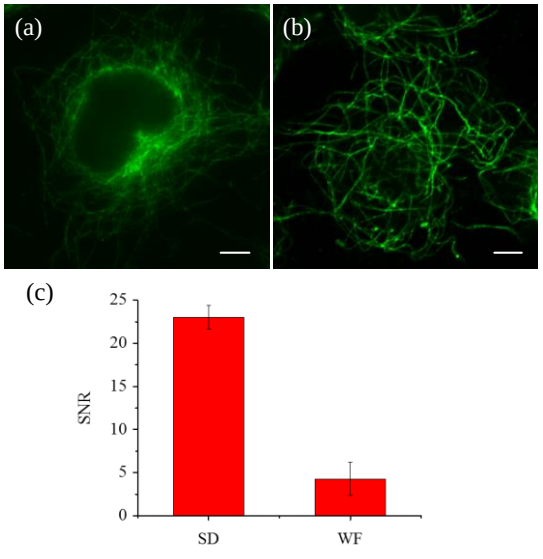

Figure 4 Quantitative analysis and comparison of SNR between (a) wide field (WF) microscopy and (b) spinning-disk (SD) confocal microscopy; (c) the SNR comparison of SD and WF images. Scale bar: (a) 10 μm and (b) 5 μm.

Straightforward 3D super-resolution imaging of SOFI was demonstrated using a wide field, lamp-based optical microscope [45], however, the SNR of wide field (WF) microscopy is much worse

than that of spinning-disk confocal microscopy, due to the lack of optical sectioning capability of wide field microscopy. Figure 4 shows that the SNR in SD microscopy can be improved by a factor of about 5 over the wide field microscopy counterpart (detail method can be seen in Fig. S3).

To determine the axial resolution enhancement, x-z cross-sections of different order SD-SOFI 3D stack were presented in Fig. 5(a-d) and intensity profiles along z direction were plotted in Fig. 5(e). The 100 frames for each slice (200 nm each slice along the z-axis) were captured for 3D SD-SOFI reconstruction and exposure time of each frame was 30 ms. As shown in Fig. 5(e), 450 nm z-resolution of spinning-disk confocal is well fitted with the relationship between SD and WF, better z-resolution was achieved when higher order SD-SOFI cumulant was used, which shows the inherent super-resolution sectioning capability of SD-SOFI.

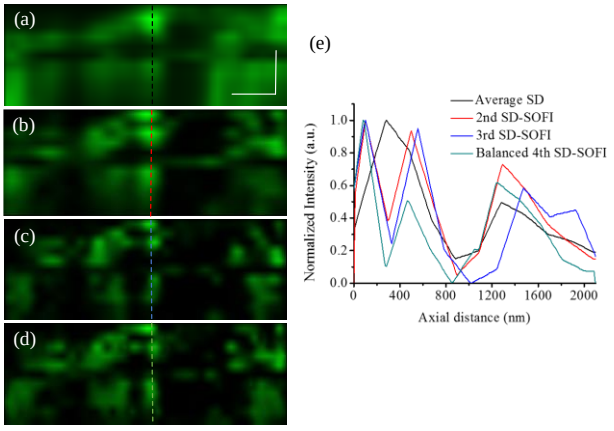

Figure 5 (a) Average SD, (b) 2nd SD-SOFI, (c) 3rd SD-SOFI, (d) balanced 4th SD-SOFI super-resolution imaging of 100 frames based on spinning-disk confocal microscope (SD) of x-z sections. (e) Vertical (x-z) cross-sections of the three-dimensional dataset plotted on dash line of (a-d). Scale bar: 1 μm.

4 Discussion

Figure 6 shows a schematic diagram of PSFs in various microscopy modalities. Wide field fluorescence microscopy usually suffers from out-of-focus blur, which worsens both the lateral and axial resolutions. Although TIRF possesses good SNR, not all biological questions are suitable to this kind of imaging system due to its limited imaging depth. Besides, TIRF lacks three-dimensional imaging capability. In spinning-disk confocal microscopy, multiple pinholes are introduced for fast imaging. The introduction of pinholes also enhances the lateral resolution and optical-sectioning capability along axial direction. However, the resolution is still limited by the diffraction. By applying SD-SOFI processing, the PSF size can be significantly reduced in all three dimensions. Moreover, higher order SD-SOFI processing generates smaller PSF, which is far below the diffraction-limited size. In SD-BaLM processing, the localization precision could be decreased down to nanometer scale, achieving a resolution of less than 30 nm. The axial resolution, however, is also constrained by the PSF of the spinning-disk confocal system[15, 47].

The optical sectioning can be provided by confocal microscopy. In comparison to conventional confocal microscopy, SD-confocal is more suitable for SOFI. In spinning disk confocal, assuming that there are N pixels on the CCD detector, and the spots of the spinning disk at the detector is N_1, then the effective dwell time for each pixel can be expressed as $(N_1/N)*T$, in which T is the frame time. In comparison, the pixel dwell time for wide-field microscopy is T, whereas a conventional confocal point scanning microscope is T/N. As the calculation of the cross-cumulants in SOFI rely on a relative long pixel dwell time t and short frame time T, we can define the temporal aspect ratio to be

$$A = t/T .$$

Therefore, the temporal aspect ratio of a spinning disk confocal microscopy ($A=N_1/N$) is comparable to the wide-field microscopy ($A=1$) for SOFI, which is much larger than the point scanning confocal microscopy ($A=1/N$). Further, the short frame time in spinning disk confocal also makes it very attractive for SD-BaLM.

However, the major limitation to 3D-SOFI, is that it relies on the blinking/fluctuation of the fluorescent label. QDs are the most popular fluorophore for SOFI, but other blinking fluorescent proteins have been used in SOFI as well [48]. Also, the resolution scaling for SOFI is linear proportional to the high-order SOFI process, which can induce

	Wide-field (λ=625nm, n=1.52, NA=1.4)	TIRF	Spinning-disk Confocal	nth order SD-SOFI	SD-BaLM
PSF_{xy} (nm)	228	228	1-$\sqrt{2}$ fold	n-$\sqrt{2n}$ fold	30
PSF_z (nm)	>970	~100	1-$\sqrt{2}$ fold	n-$\sqrt{2n}$ fold	1-$\sqrt{2}$ fold

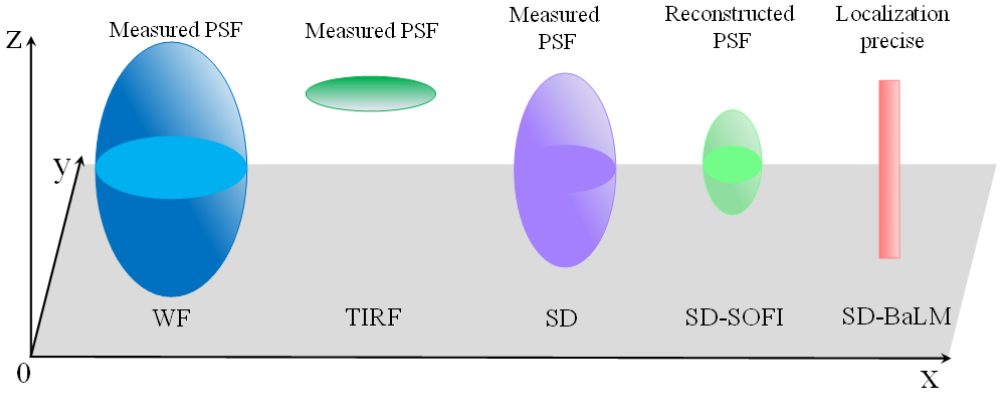

Figure 6 Illustration of the resolution scaling for different methods. As can be seen, SD-confocal can provide up to 1.4-fold of resolution enhancement depending on the pinhole size, in addition to the optical sectioning. The nth order SOFI can provide n fold resolution scaling. Therefore, SD-SOFI can provide super-resolution $\sqrt{2}$ n fold that of diffraction limited WF microscopy, in both lateral and axial resolution. Although SD-BaLM can provide precise localization, its axial resolution is limited by the spinning disk confocal.

artifact. In this work, we have used 100 frames for each layer of SD-SOFI reconstruction, which takes 3 seconds. With the blinking enhanced QD, the temporal resolution could be improve by 10-fold, or with 10 frames only [49].

For 3D-BaLM, the ratio of bleaching/blinking has to be controlled to less than 1 bleaching/blinking molecule per PSF area per pixel dwell time, to guarantee the localization precision. There are two parameters involved: the bleaching/blinking ratio (temporal criterion), and the labeling density (spatial criterion). Too fast bleaching/blinking ratio can cause error (overlapped emission within one pixel dwell time) in localization in BaLM, while too slow bleaching/blinking requires much more frames for reconstruction.

Meanwhile, a relative low labelling density can ease both SOFI and BALM from possible redundant overlapping molecules toward artifact. However, a high labeling density ensures the fidelity of the final image to reflect the subcellular structure. Recently, we have introduced joint-tagging SOFI, namely using QDs with different spectrums, to circumvent this problem through simultaneous multi-spectral channel detection. In each channel, the labeling density is relatively low, whereas the sum-up labeling density of multiple channels is high enough to reflect the structure in greater details [50].

5 Conclusions

Previous super-resolution techniques require complicated setup to achieve three-dimensional super-resolution, which limits their wide application. Taking advantage of the 3D optical sectioning capability of spinning disk confocal microscopy, we describe a 3D-multimodal sub-diffraction imaging with spinning-disk confocal microscopy (3D-MUSIC) using fluctuation probes, which makes use of the intrinsic fluctuation behavior of the fluorescent probes.

Although the spatial resolution of 3D-MUSIC may be the inherent weakness when comparing with other single-molecule localization-based super-resolution techniques, the advantages of 3D-MUSIC could be summarized: (1) time

resolution is much better than conventional localization super-resolution techniques; (2) the simplicity and practicality that without special requirement of engineered photon-switchable or photo-activated fluorescent proteins, although these probes should also work as well; (3) excellent signal-to-noise ratio and 3D optical-sectioning ability using spinning-disk confocal microscopy; (4) allowing better intracellular super-resolution compare with TIRF or wide field. It's hopeful to combine 3D-MUSIC with compressive sensing to improve both time and spatial resolution and achieve super-resolution images *in vivo* due to its excellent 3D optical-sectioning ability and better temporal resolution. Also, it should be noted that, the application of 3D-MUSIC is not restricted on QD as the fluorescent label, other blinking/fluctuation dyes such as photo-switchable fluorescent proteins [40], carbon nanodots [51, 52], and nitrogen-vacancy centres in fluorescent nanodiamond [53], are also suitable to this method.

Acknowledgements

This work was supported by the National Instrumentation Program (2013YQ03065102), the "973" Major State Basic Research Development Program of China (2011CB809101, 2010CB933901), and the National Natural Science Foundation of China (61178076, 31327901, 61475010).

Electronic Supplementary Material:
Supplementary material (Cell preparation, Comparisons of simulation results with noise, SNR calculation of Fig. 4) is available in the online version of this article at http://dx.doi.org/10.1007/s12274-***-****-*.

References

[1] Giloh, H.; Sedat, J. W. Fluorescence microscopy: reduced photobleaching of rhodamine and fluorescein protein conjugates by n-propyl gallate. *Science* **1982**, *217*, 1252-1255.

[2] Baschong, W.;Suetterlin, R.; Laeng, R. H. Control of autofluorescence of archival formaldehyde-fixed, paraffin-embedded tissue in confocal laser scanning microscopy (CLSM). *Journal of Histochemistry & Cytochemistry* **2001**, *49*, 1565-1571.

[3] Carlsson, K.;Danielsson, P.-E.;Liljeborg, A.;Majlöf, L.;Lenz, R.; Åslund, N. Three-dimensional microscopy using a confocal laser scanning microscope. *Optics Letters* **1985**, *10*, 53-55.

[4] Wang, Y.;Kuang, C.;Cai, H.;Li, S.;Liu, W.;Hao, X.;Ge, J.; Liu, X. Sub-diffraction imaging with confocal fluorescence microscopy by stochastic photobleaching. *Optics Communications* **2014**, *312*, 62-67.

[5] Tanaami, T.;Otsuki, S.;Tomosada, N.;Kosugi, Y.;Shimizu, M.; Ishida, H. High-speed 1-frame/ms scanning confocal microscope with a microlens and Nipkow disks. *Applied Optics* **2002**, *41*, 4704-4708.

[6] Conchello, J.-A.; Lichtman, J. W. Optical sectioning microscopy. *Nature methods* **2005**, *2*, 920-931.

[7] Gligorijevic, B.;Purdy, K.;Elliott, D. A.;Cooper, R. A.; Roepe, P. D. Stage independent chloroquine resistance and chloroquine toxicity revealed via spinning disk confocal microscopy. *Molecular and biochemical parasitology* **2008**, *159*, 7-23.

[8] Gligorijevic, B.;Bennett, T.;McAllister, R.;Urbach, J. S.; Roepe, P. D. Spinning disk confocal microscopy of live, intraerythrocytic malarial parasites. 2. Altered vacuolar volume regulation in drug resistant malaria. *Biochemistry* **2006**, *45*, 12411-12423.

[9] Egeblad, M.;Ewald, A. J.;Askautrud, H. A.;Truitt, M. L.;Welm, B. E.;Bainbridge, E.;Peeters, G;Krummel, M. F.; Werb, Z. Visualizing stromal cell dynamics in different tumor microenvironments by spinning disk confocal microscopy. *Disease models & mechanisms* **2008**, *1*, 155-167.

[10] Sisan, D. R.;Arevalo, R.;Graves, C.;McAllister, R.; Urbach, J. S. Spatially resolved fluorescence correlation spectroscopy using a spinning disk confocal microscope. *Biophysical journal* **2006**, *91*, 4241-4252.

[11] Cox, G; Sheppard, C. J. Practical limits of resolution in confocal and non - linear microscopy. *Microscopy research and technique* **2004**, *63*, 18-22.

[12] Mart ínez-Corral, M.;Andres, P.;Ojeda-Castaneda, J.; Saavedra, G. Tunable axial superresolution by annular binary filters. Application to confocal microscopy. *Optics communications* **1995**, *119*, 491-498.

[13] Nagorni, M.; Hell, S. W. 4Pi-confocal microscopy provides three-dimensional images of the microtubule network with 100-to 150-nm resolution. *Journal of structural biology* **1998**, *123*, 236-247.

[14] Huang, B.;Bates, M.; Zhuang, X. Super resolution fluorescence microscopy. *Annual review of biochemistry* **2009**, *78*, 993.

[15] Schermelleh, L.;Heintzmann, R.; Leonhardt, H. A guide to super-resolution fluorescence microscopy. *The Journal of cell biology* **2010**, *190*, 165-175.

[16] Hell, S. W. Far-field optical nanoscopy. *science* **2007**, *316*, 1153-1158.

[17] Hell, S. W. Toward fluorescence nanoscopy. *Nature Biotechnology* **2003**, *21*, 1347-1355.

[18] Baddeley, D.;Cannell, M. B.; Soeller, C. Three-dimensional sub-100 nm super-resolution imaging of biological samples using a phase ramp in the objective pupil. *Nano Research* **2011**, *4*, 589-598.

[19] Hell, S. W.; Wichmann, J. Breaking the diffraction resolution limit by stimulated emission: stimulated-emission-depletion fluorescence microscopy. *Optics letters* **1994**, *19*, 780-782.

[20] Klar, T. A.;Jakobs, S.;Dyba, M.;Egner, A.; Hell, S. W. Fluorescence microscopy with diffraction resolution barrier broken by stimulated emission. *Proceedings of the National Academy of Sciences* **2000**, *97*, 8206-8210.

[21] Gustafsson, M. G. Nonlinear structured-illumination microscopy: wide-field fluorescence imaging with theoretically unlimited resolution. *Proceedings of the National Academy of Sciences of the United States of America* **2005**, *102*, 13081-13086.

[22] Rego, E. H.;Shao, L.;Macklin, J. J.;Winoto, L.;Johansson, G. A.;Kamps-Hughes, N.;Davidson, M. W.; Gustafsson, M. G. Nonlinear structured-illumination microscopy with a photoswitchable protein reveals cellular structures at 50-nm resolution. *Proceedings of the National Academy of Sciences* **2012**, *109*, E135-E143.

[23] Shroff, H.;Galbraith, C. G.;Galbraith, J. A.; Betzig, E. Live-cell photoactivated localization microscopy of nanoscale adhesion dynamics. *Nature Methods* **2008**, *5*, 417-423.

[24] Manley, S.;Gillette, J. M.;Patterson, G. H.;Shroff, H.;Hess, H. F.;Betzig, E.; Lippincott-Schwartz, J. High-density mapping of single-molecule trajectories with photoactivated localization microscopy. *Nature methods* **2008**, *5*, 155-157.

[25] Rust, M. J.;Bates, M.; Zhuang, X. Sub-diffraction-limit imaging by stochastic optical reconstruction microscopy (STORM). *Nature methods* **2006**, *3*, 793-796.

[26] Huang, B.;Wang, W.;Bates, M.; Zhuang, X. Three-Dimensional Super-Resolution Imaging by Stochastic Optical Reconstruction Microscopy. *Science* **2008**, *319*, 810-813.

[27] Burnette, D. T.;Sengupta, P.;Dai, Y.;Lippincott-Schwartz, J.; Kachar, B. Bleaching/blinking assisted localization microscopy for superresolution imaging using standard fluorescent molecules. *Proceedings of the National Academy of Sciences* **2011**, *108*, 21081-21086.

[28] Dertinger, T.;Colyer, R.;Iyer, G.;Weiss, S.; Enderlein, J. Fast, background-free, 3D super-resolution optical fluctuation imaging (SOFI). *Proceedings of the National Academy of Sciences* **2009**, *106*, 22287-22292.

[29] Dertinger, T.;Colyer, R.;Vogel, R.;Enderlein, J.; Weiss, S. Achieving increased resolution and more pixels with Superresolution Optical Fluctuation Imaging (SOFI). *Optics Express* **2010**, *18*, 18875-18885.

[30] Pavani, S. R. P.;Thompson, M. A.;Biteen, J. S.;Lord, S. J.;Liu, N.;Twieg, R. J.;Piestun, R.; Moerner, W. Three-dimensional, single-molecule fluorescence imaging beyond the diffraction limit by using a double-helix point spread function. *Proceedings of the National Academy of Sciences* **2009**, *106*, 2995-2999.

[31] Yuen, H. P. Two-photon coherent states of the radiation field. *Physical Review A* **1976**, *13*, 2226.

[32] Geissbuehler, S.;Bocchio, N. L.;Dellagiacoma, C.;Berclaz, C.;Leutenegger, M.; Lasser, T. Mapping molecular statistics with balanced super-resolution optical fluctuation imaging (bSOFI). *Optical Nanoscopy* **2012**, *1*, 1-7.

[33] Leutwyler, W. K.;Bürgi, S. L.; Burgl, H. Semiconductor clusters, nanocrystals, and quantum dots. *Science* **1996**, *271*, 933-937.

[34] Xie, R.;Chen, K.;Chen, X.; Peng, X. InAs/InP/ZnSe core/shell/shell quantum dots as near-infrared emitters: bright, narrow-band, non-cadmium containing, and biocompatible. *Nano research* **2008**, *1*, 457-464.

[35] Dertinger, T.;Heilemann, M.;Vogel, R.;Sauer, M.; Weiss, S. Superresolution optical fluctuation imaging with organic dyes. *Angewandte Chemie* **2010**, *122*, 9631-9633.

[36] Chang, H.;Zhang, M.;Ji, W.;Chen, J.;Zhang, Y.;Liu, B.;Lu, J.;Zhang, J.;Xu, P.; Xu, T. A unique series of reversibly switchable fluorescent proteins with beneficial properties for various applications. *Proceedings of the National Academy of Sciences* **2012**, *109*, 4455-4460.

[37] Habuchi, S.;Ando, R.;Dedecker, P.;Verheijen, W.;Mizuno, H.;Miyawaki, A.; Hofkens, J. Reversible single-molecule photoswitching in the GFP-like fluorescent protein Dronpa. *Proceedings of the National Academy of Sciences of the United States of America* **2005**, *102*, 9511-9516.

[38] Michalet, X.;Pinaud, F. F.;Bentolila, L. A.;Tsay, J. M.;Doose, S.;Li, J. J.;Sundaresan, G.;Wu, A. M.;Gambhir, S. S.; Weiss, S. Quantum dots for live cells, in vivo imaging, and diagnostics. *Science* **2005**, *307*, 538-544.

[39] Kairdolf, B. A.;Smith, A. M.;Stokes, T. H.;Wang, M. D.;Young, A. N.; Nie, S. Semiconductor quantum dots for bioimaging and biodiagnostic applications. *Annual Review of Analytical Chemistry* **2013**, *6*, 143-162.

[40] Xu, J.;Chang, J.;Yan, Q.;Dertinger, T.;Bruchez, M. P.; Weiss, S. Labeling cytosolic targets in live cells with blinking probes. *The journal of physical chemistry letters* **2013**, *4*, 2138-2146.

[41] Guizar-Sicairos, M.;Thurman, S. T.; Fienup, J. R. Efficient subpixel image registration algorithms. *Optics letters* **2008**, *33*, 156-158.

[42] Geissbuehler, S.;Dellagiacoma, C.; Lasser, T. Comparison between SOFI and STORM. *Biomedical optics express* **2011**, *2*, 408-420.

[43] Henriques, R.;Lelek, M.;Fornasiero, E. F.;Valtorta, F.;Zimmer, C.; Mhlanga, M. M. QuickPALM: 3D real-time photoactivation nanoscopy image processing in ImageJ. *Nature methods* **2010**, *7*, 339-340.

[44] Maglione, M.; Sigrist, S. J. Seeing the forest tree by tree: super-resolution light microscopy meets the neurosciences. *Nature neuroscience* **2013**, *16*, 790-797.

[45] Dertinger, T.;Xu, J.;Naini, O. F.;Vogel, R.; Weiss, S. SOFI-based 3D superresolution sectioning with a widefield microscope. *Optical nanoscopy* **2012**, *1*, 1-5.

[46] Pawley, J. *Handbook of biological confocal microscopy*; Springer, 2010.

[47] Ding, Y.;Xi, P.; Ren, Q. Hacking the optical diffraction limit: Review on recent developments of fluorescence nanoscopy. *Chinese Science Bulletin* **2011**, *56*, 1857-1876.

[48] Dedecker, P.;Mo, G. C.;Dertinger, T.; Zhang, J. Widely accessible method for superresolution fluorescence imaging of living systems. *Proceedings of the National Academy of Sciences* **2012**, *109*, 10909-10914.

[49] Watanabe, T. M.;Fukui, S.;Jin, T.;Fujii, F.; Yanagida, T. Real-time nanoscopy by using blinking enhanced quantum dots. *Biophysical journal* **2010**, *99*, L50-L52.

[50] Zeng, Z.;Chen, X.;Wang, H.;Huang, N.;Shan, C.;Zhang, H.;Teng, J.; Xi, P. Fast Super-Resolution Imaging with Ultra-High Labeling Density Achieved by Joint Tagging Super-Resolution Optical Fluctuation Imaging. *Scientific Reports* **2015**, *5*, 8359.

[51] Das, S. K.;Liu, Y.;Yeom, S.;Kim, D. Y.; Richards, C. I.

Single-Particle Fluorescence Intensity Fluctuations of Carbon Nanodots. *Nano letters* **2014**, *14*, 620-625.

[52] Liu, Q.;Guo, B.;Rao, Z.;Zhang, B.; Gong, J. R. Strong two-photon-induced fluorescence from photostable, biocompatible nitrogen-doped graphene quantum dots for cellular and deep-tissue imaging. *Nano letters* **2013**, *13*, 2436-2441.

[53] Bradac, C.;Gaebel, T.;Naidoo, N.;Sellars, M.;Twamley, J.;Brown, L.;Barnard, A.;Plakhotnik, T.;Zvyagin, A.; Rabeau, J. Observation and control of blinking nitrogen-vacancy centres in discrete nanodiamonds. *Nature nanotechnology* **2010**, *5*, 345-349.

Electronic Supplementary Material

Three dimensional multimodal sub-diffraction imaging with spinning-disk confocal microscopy using blinking/fluctuation probes

Xuanze Chen†, Zhiping Zeng†, Hening Wang, and Peng Xi (✉)

Department of Biomedical Engineering, College of Engineering, Peking University, Beijing 100871, China
† *Authors with equal contribution*

Supporting information to DOI 10.1007/s12274-****-****-* (automatically inserted by the publisher)

Cell preparation

COS7 African green monkey fibroblast cells were seeded on glass cover slides for overnight growth. Before staining, cells were washed with 1X PBS buffer, and extracted with 0.2% Triton X-100 for 1 min in a pH 7 buffer consisting of 0.1 M PIPES, 1 mM ethylene glycol tetraacetic acid, and 1 mM magnesium chloride. Subsequently, the cells were fixed with 4% paraformaldehyde and 0.1% glutaraldehyde in PBS for 10 min. Reduction was carried out with 1mg/ml $NaBH_4$ in water for 5 min and then wash with PBS. The cells were blocked and permeabilized with 5% bovine serum albumin (Jackson ImmunoResearch Laboratories) and 0.5% v/v Triton X-100 in PBS for 30 min. After blocking and permeabilization, anti-alpha tubulin primary antibody with biotin (ab74696, Abcam) was diluted to 10 μg/mL in blocking buffer and added to cells for 40 min. After washing with PBS, cells were stained for1 h with QDs streptavidin conjugates (Invitrogen) with emission peak at 625 nm, and QDs were diluted to 15nM in blocking buffer. Then cells were washed with PBS for 3 times, 5 minutes each. Finally a post-fixation was implemented in a mixture of 4% formaldehyde and 0.1% glutaraldehyde in PBS for 10 min. Finally, the cells were washed and mounted with 50% glycerin.

Address correspondence to xipeng@pku.edu.cn

Correlation coefficients of the target image with the average, SD-SOFI and SD-BaLM.

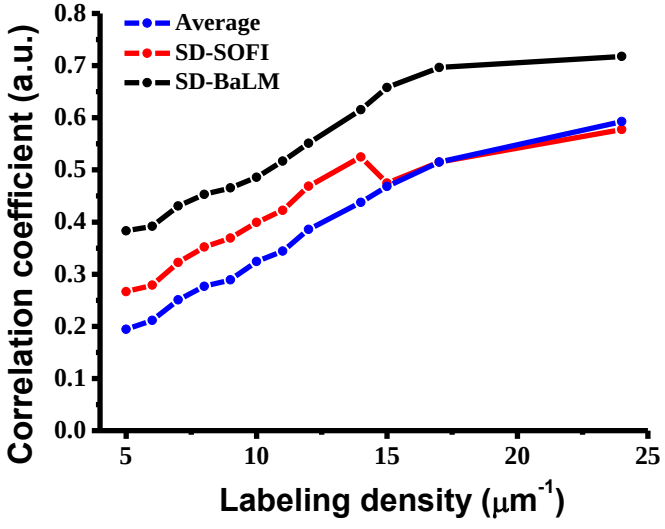

Figure S1 The curves describing the correlation coefficients of the target image with the average, SD-SOFI and SD-BaLM. The correlation coefficients augment with the increase of labeling densities for the average, SD-SOFI and SD-BaLM results. Therefore, the labeling densities should be sufficiently high for guaranteeing the fidelity of the reconstructed images.

Comparisons of simulation results with and without noise.

To test the noise resistance and robustness of the proposed multimodal method, a random noise was taken into consideration in the subsequent simulations. The noise distribution was generated by using uniformly distributed random numbers, which simulates the dark-current noise of the detector, with SNR of 4 in each frame of image sequences. In Fig. S2 (e), the test object was interfered with random noise. After image averaging shown in Fig. S2 (f), the noise can be suppressed. However, the test object cannot be well distinguished due to the diffraction limit. In Fig. S2 (g), apparently, SD-SOFI processing has improved the resolution and further eliminated the background noise. After SD-BaLM processing, the test object can be clearly visualized and the background noise was largely suppressed as well.

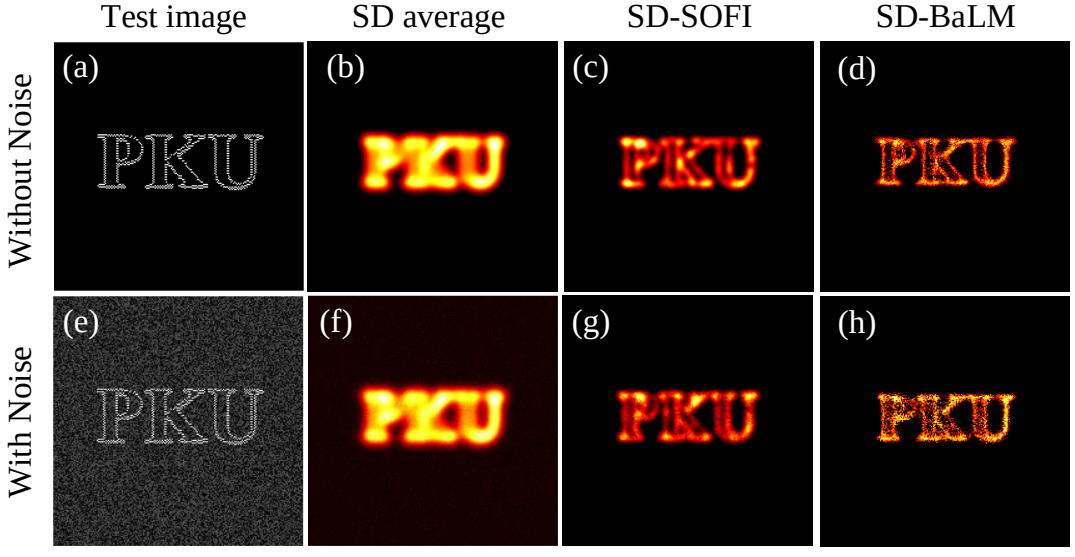

Figure S2 Comparisons of simulation results with and without adding noise. (a) The test image; (b) the average spinning-disk confocal image of 1000 test images; (c) the retrieved spinning-disk confocal SOFI image from 1000 frames without noise (3rd cumulant SD-SOFI); (d) the retrieved SD-BaLM images from 1000 frames without noise; (e-h) the corresponding images of (a-d) with random noise.

Signal to noise ratio estimation.

The SNR was estimated by calculating the amplitude ratio between the signal and the background noise, i.e., $SNR = \frac{A_{signal}}{A_{noise}}$. In Figs. 4(a) and 4(b), firstly we selected a ROI (using the command 'roipoly' in Matlab) which has uniform noise fluctuation. Then the noise distribution was calculated by computing the histogram of the pixels in the ROI as shown in Fig. S3. The average value in the ROI was regarded as the noise amplitude A_{noise}. Subsequently, a ROI which contains dominant signal information was selected, then the average signal value was assigned as the signal amplitude A_{signal}. Consequently, the SNR can be estimated by calculating the ratio between A_{signal} and A_{noise}. After calculation, the SNRs for wide-field and spinning-disk confocal images are 4.3 and 23, respectively.

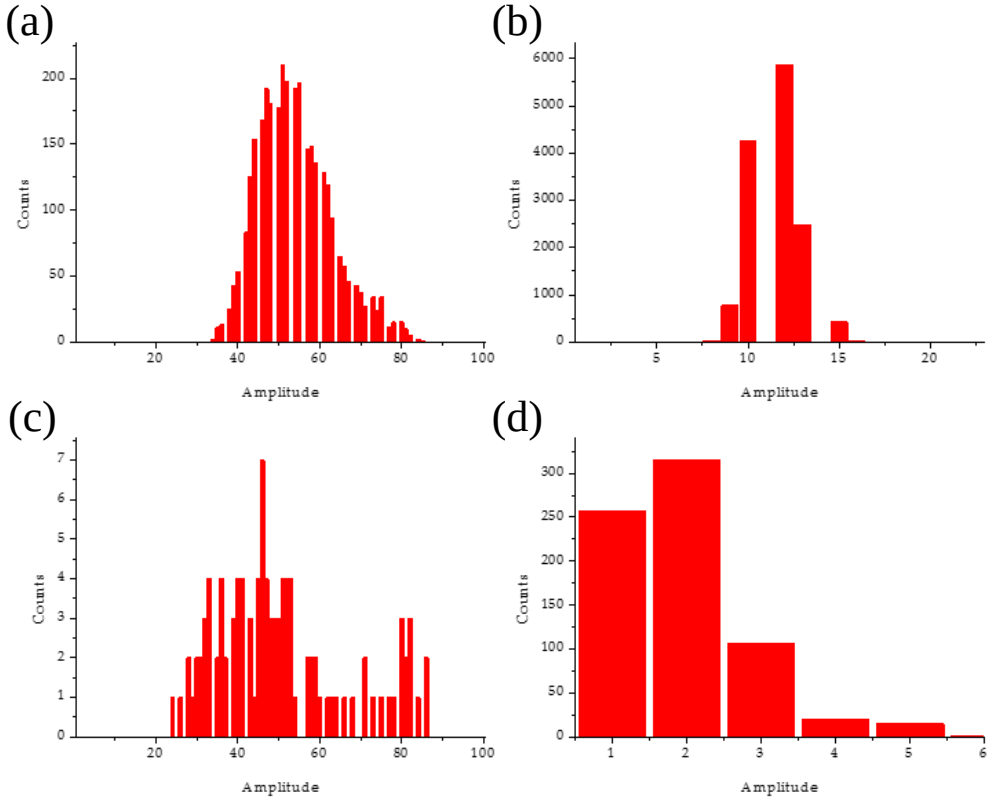

Figure S3 (a) Signal amplitude distribution of wide-field image. (b) Noise amplitude distribution of wide-field image. (c) Signal amplitude distribution of spinning-disk confocal image. (d) Noise amplitude distribution of spinning-disk confocal image.

MOVIE S-1 Three-dimensional spinning disk confocal microscopy reconstructed images of the microtubules in COS7 cells (shown in Fig. 5(a))

MOVIE S-2 Three-dimensional balanced 4th SD-SOFI reconstructed images of the microtubules in COS7 cells (shown in Fig. 5(d))